scientific reports

Check for updates

OPEN

Major individual and regional variations in unit entrainment by oscillations of different frequencies

Mohamed Badawy[1], Ian T. Kim[1], Alon Amir[1], Mohammad M. Herzallah[1,3], Luisa F. Gomez-Alatorre[1], Drew B. Headley[1] & Denis Paré[1,2]✉

In vitro studies have shown that a neuron's electroresponsive properties can predispose it to oscillate at specific frequencies. In contrast, network activity in vivo can entrain neurons to rhythms that their biophysical properties do not predispose them to favor. However, there is limited information on the comparative frequency profile of unit entrainment across brain regions. Therefore, this study aimed to characterize the frequency profile of unit entrainment in cortex, thalamus, striatum, and basolateral amygdala (BLA) in rats of either sex. Neurons recorded simultaneously in a given brain region and behavioral state generally had very similar frequency profiles of unit entrainment. While cortical, striatal, and thalamic neurons were more strongly entrained by low than high local field potential (LFP) frequencies, increases in the power of these oscillations were linked to decreased firing rates for low frequencies versus increased firing rates for high frequencies. Deviating from this general trend, BLA neurons were more strongly entrained by high gamma than all other frequency bands in all subjects and states. By contrast, neurons in other regions displayed marked inter-individual variability. That is, although neurons in some regions had exceptionally high entrainment values in particular frequency bands, these were not observed consistently across rats. Based on these findings, some might infer that oscillations play a minor role or that different oscillatory patterns can support the same functions. Alternatively, the oscillations critical to brain function could be those not investigated here, namely those arising transiently in response to specific task variables or contexts. Perhaps those are less susceptible to genetic variations. While our findings do not allow us to determine which explanation is correct, they do highlight the perils of averaging.

Keywords Oscillations, Local field potentials, Entrainment, Inter-individual variability, Amygdala

Neuronal networks generate rhythmic population events, measurable in local field potentials (LFPs) as oscillations of various frequencies. Understanding oscillations is important because brain computations depend on neuronal interactions that are embedded in these population rhythms[1]. Oscillations provide an energy efficient way to coordinate interactions within and between networks: by producing alternating periods of enhanced and lowered neuronal excitability, they telescope epochs of effective synaptic interactions into short recurring time windows.

Oscillations of various frequencies occur in different brain regions and as a function of behavioral states, with the same or different networks exhibiting multiple interacting rhythms. Generally, one observes a $1/f^n$ attenuation of oscillatory power with increases in frequency because low frequency rhythms generate synchronized membrane potential variations of high amplitude in widely distributed neurons, whereas high frequency oscillations correlate with low amplitude membrane potential fluctuations that involve fewer cells[2,3].

When different groups of cells oscillate at the same frequency, coordinated synaptic interactions are believed to depend on the coherence of the oscillating groups of neurons[4].When neurons oscillate at different frequencies, coordination may depend on phase-amplitude coupling, when the phase of the slower oscillation is associated with rhythmic changes in the power of the faster oscillation[5], or phase coupling, when the frequency of two oscillations exhibit a rational dependence[6].

How do neuronal oscillations arise? At the single cell level, in vitro studies revealed that due to differences in their passive properties and complement of voltage-gated conductances, different types of neurons exhibit

[1]Center for Molecular and Behavioral Neuroscience, Rutgers University, Newark, NJ 07102, USA. [2]Center for Molecular & Behavioral Neuroscience, Rutgers University-Newark, 197 University Avenue, Newark, NJ 07102, USA. [3] Palestinian Neuroscience Initiative, Al-Quds University, Jerusalem, Palestine. ✉email: pare@rutgers.edu

resonance at specific frequencies, for which they exhibit a preferential responsiveness[7]. Moreover, some resonant neurons generate self-sustained, intrinsic membrane potential oscillations near the resonant frequency[8].

What happens when such intrinsically oscillating or resonating neurons are inserted in an intact network? In some cases, they promote the emergence and propagation of large-scale coherent oscillations at the corresponding frequency through rhythmic interactions with their synaptic partners. Well documented examples of this include thalamocortical cells whose capacity to generate intrinsic oscillations in the 1–4 Hz range[9] is thought to contribute to the emergence of widespread delta oscillations across the thalamocortical network during slow-wave sleep (SWS). However, even in this extreme case, network interactions can at times shift emergent oscillatory activity to a different frequency, leading to the occurrence of sleep spindles in the 7–14 Hz range[10].

In fact, many deviations between resonant and preferred firing frequencies have been documented. For instance, principal neurons of the basolateral amygdala (BLA) exhibit intrinsic voltage-dependent oscillatory activity and resonance at around 4–10 Hz[11–14]. Yet, these cells are preferentially entrained by LFP rhythms in the high-gamma range[15]. Moreover, fast-spiking BLA interneurons show the same frequency preference, despite having strikingly different electroresponsive properties[16–19]. Overall, the above indicates that although intrinsic electroresponsive properties bias neuronal activity, network activity can overcome this intrinsic preference and cause neurons to entrain to rhythms that their biophysical properties do not predispose them to favor.

At present, there is limited information on the comparative frequency profile of unit entrainment across brain regions because investigators have generally focused on specific rhythms in one or a few connected regions in relation to task events. Therefore, the present study was undertaken to characterize the frequency profile of unit entrainment in a vast array of brain regions, including cortical, thalamic, striatal, and BLA neurons. In all these brain regions except the BLA, neurons were more strongly entrained by low than high LFP frequencies even though increases in the power of these oscillations were linked to decreased firing rates for low frequencies versus increased firing rates for high frequencies. Unexpectedly, we observed marked inter-individual differences in the frequency profile of unit entrainment in all investigated regions except for the BLA.

Results

We aimed to determine whether LFP rhythms of distinct frequencies differentially entrain various types of neurons, a property termed "frequency profile of unit entrainment". Cortical ($n = 1307$; Table 1), thalamic ($n = 1705$; Table 1), striatal ($n = 303$), and BLA neurons ($n = 573$) were recorded with Neuropixel or silicon probes in 23 rats (18 males and 5 females). Cortical recordings were obtained from functionally diverse regions. Most thalamic neurons were recorded in midline thalamic nuclei. Striatal recordings were obtained dorsal to the amygdala. We first describe the approach used in a single cell type and then apply it to various types of neurons recorded during SWS, quiet wakefulness (QW), and task performance (see Methods).

General approach

To calculate the frequency profile of unit entrainment, we related the spike times of each unit to LFPs recorded 200 µm away, thereby avoiding spectral leakage of spike waveforms into LFPs[20,21]. For each cell, we bandpass filtered the LFP for a specific frequency band, measured the magnitude of entrainment (resultant vector, R) and preferred phase (Fig. S1), and then averaged the results obtained across all simultaneously recorded neurons in a given region.

The frequency profile of unit entrainment of 41 neurons recorded simultaneously in the interanteromedial thalamic nucleus during SWS is shown in Fig. 1a. To examine the relation between LFP power and firing rate, we computed LFP power (Fig. 1b, y-axis) for the different frequency bands (x-axis) in one-second windows sliding in steps of 200 ms, and color coded the cells' z-scored firing rates for each frequency-power bin (Fig. 1b, top).

Cortical areas			Thalamic nuclei		
	Units	Rats		Units	Rats
S1	372	6	Anteromedial	79	3
Anterior insula	147	3	Central medial	959	9
Anterior cingulate	91	3	Interanteromedial	68	2
Prelimbic	214	3	Mediodorsal	165	4
Infralimbic	152	4	Paracentral	105	2
Dorsal peduncular	140	4	Paraventricular	31	1
Taenia tecta	60	4	Reuniens	68	1
Retrosplenial	70	2	Rhomboid	24	1
Subiculum	61	1	Submedius	152	4
			Ventral lateral	54	2
Total	**1307**			1705	

Table 1. Locations of cortical and thalamic neurons recorded in this study. Neurons were recorded in 23 rats implanted with one to four neuropixel or silicon probes. Cortical recordings were obtained from functionally diverse regions. Most thalamic neurons were recorded in midline thalamic nuclei. Striatal recordings were obtained dorsal to the amygdala ($n = 303$). Part of the BLA ($n = 573$) and thalamic recordings were previously used to analyze the neuronal correlates of foraging behavior[17,73].

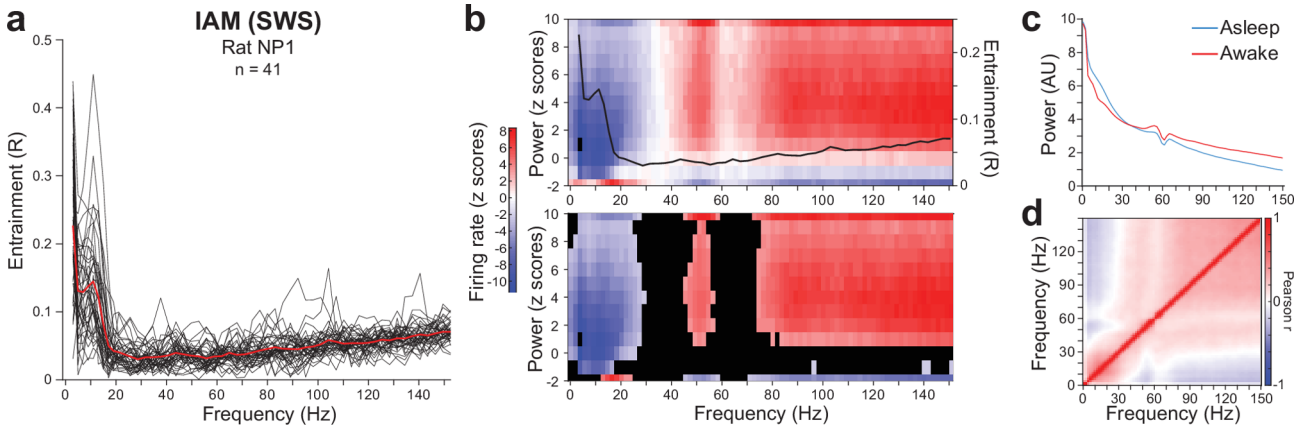

Fig. 1. Approach to analyses. (**a**) Frequency profile of unit entrainment for a representative group of 41 neurons recorded simultaneously in a single subject in the interanteromedial thalamic nucleus during SWS. Black lines: individual cells. Red line: average. (**b**, **top**) Relation between LFP power (left y-axis), frequency (x-axis), firing rate (color bar), and entrainment (black line, right y-axis) in the same group of cells. LFP power for different frequency bands was computed in windows of one second sliding in steps of 200 ms and z-scored. The z-scored firing rate of the cells is color coded for each frequency-power bin. (**b**, **bottom**) Significant bin clusters have the same color as in the top panel whereas non-significant bins are black. (**c**) Fast Fourier transform of the corresponding LFPs. (**d**) Correlation between power in different frequency bands.

This analysis generally revealed that firing rates increased with power up to ~4–6 z-score, except for a range of low frequencies (up to 15–30 Hz) where firing rate decreased with power. Next, we determined the maximum size of bin clusters that could be obtained by chance using shifted spike train distributions (see Methods). In Fig. 1b (bottom), clusters of significant bins that exceeded that size at $p \leq 0.01$ are colored whereas insignificant ones are black.

To determine if peaks in the frequency profile of unit entrainment were associated with increased spectral power at the same frequency, we computed a Fast Fourier Transform (FFT) of the corresponding LFPs (Fig. 1c). We also correlated LFP power in different frequency bands (Fig. 1d), which generally revealed that the power of low (< 30 Hz) and high frequency rhythms were negatively correlated.

State dependence of unit entrainment

Applying this approach to neurons recorded in different brain regions revealed several common trends and some unexpected deviations. Among the former, irrespective of behavioral state, cortical, thalamic, and striatal neurons were most strongly entrained by low LFP frequencies, particularly in the delta range (Fig. 2a–c; statistics in figure legend). By contrast, BLA neurons were more strongly entrained by high-gamma than all other frequencies (Fig. 2d). Second, entrainment by low frequencies was higher in SWS than QW or during task performance, a result that also applied to BLA cells.

Generally, neurons recorded simultaneously in a given brain region and behavioral state had a similar frequency profile of unit entrainment. Moreover, the entrainment profiles of presumed principal cells and fast-spiking interneurons were also similar (classification criteria in Methods). To quantify this, we correlated the entrainment values of all cell pairs in eight cortical regions in which we had data from two or more rats (range 2–6; Fig. 2e). We then compared the average correlations within versus between cell types (statistics in figure legend). In cortical neurons, the correlation was slightly but significantly higher in pairs of interneurons than principal cells in all three states. However, the magnitude of this effect (partial eta squared = 0.002) was much lower than that of the behavioral state (partial eta squared = 0.026), with correlations within and between cell types being much higher in SWS than QW or task performance. Performing the same analyses in BLA neurons (Fig. 2f) also revealed that the effect of state was much larger than cell type identity. However, in this case, QW, not SWS, was associated with the highest correlation.

Relation between firing rate and entrainment as a function of LFP frequency

Although cortical, thalamic, and striatal neurons were more strongly entrained by low than high LFP frequencies, increases in the power of low LFP frequencies were generally associated with decreased firing rates. Conversely, high LFP frequencies were usually associated with lower entrainment but higher firing rates (Fig. 3 where non-significant bins are black). Stated otherwise, although these neurons were more strongly entrained by low than high LFP frequencies, rises in the power of low versus high LFP frequencies were generally associated with decreased versus increased firing rates, respectively. Depending on the structure and behavioral state, the range of low or high frequencies associated with significant decreases or increases in firing rates varied markedly. Among the various cases in Fig. 3, the upper limit of the LFP frequency range associated with decreased firing rates varied between ~ 15 and 30 Hz.

There were also pronounced differences in cell-to-cell variations between states. To quantify this heterogeneity, we correlated the 3D graphs' bin values between all pairs of cells and then compared the distributions of *r*

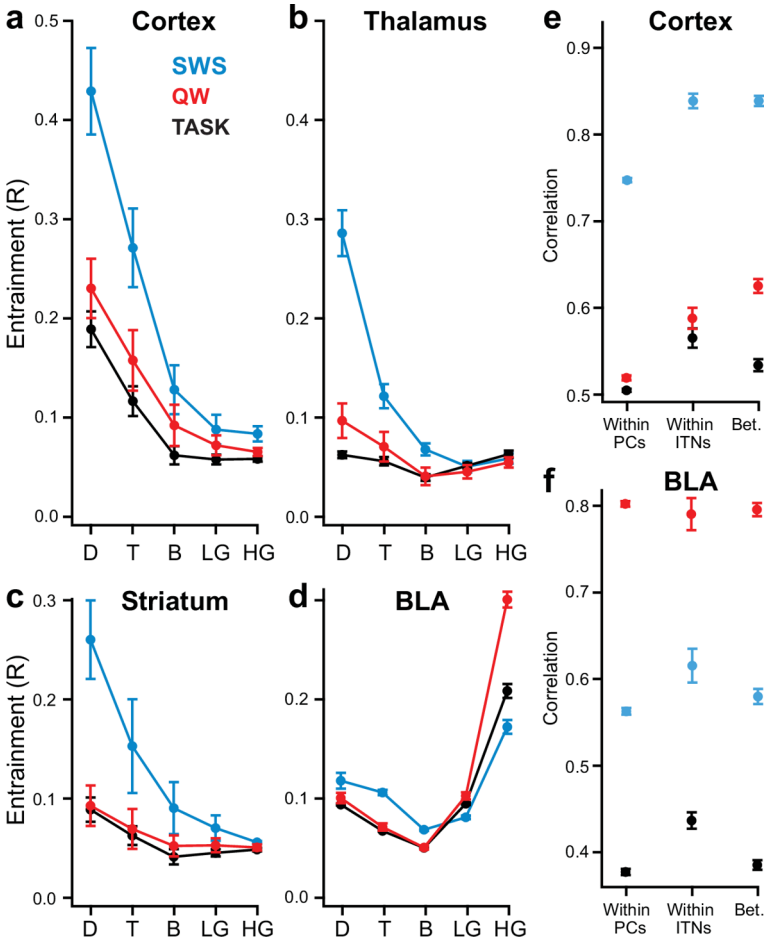

Fig. 2. State-dependence of unit entrainment. Resultant vector (y-axis) as a function of frequency band (x-axis; D, delta; T, Theta; B, Beta; LG, low-gamma; HG, high-gamma) for cortical (**a**), thalamic (**b**), striatal (**c**), and BLA (**d**) neurons. SEMs are based on the number of rats. (**a**) 1307 neurons from nine cortical areas recorded in 1–5 rats. (**b**) 1705 neurons recorded from ten nuclei in 1–9 rats. (**c**) 303 neurons recorded in seven rats. (**d**) 573 neurons recorded in seven rats. Mixed-model ANOVA revealed a significant effect of between-subject variables brain structure ($df = 3$, $F = 19.16$, $p < 0.0001$), and state ($df = 2$, $F = 18.59$, $p < 0.0001$) and of within-subject variable frequency band ($df = 4$, $F = 64.59$, $p < 0.0001$). Variables exhibited multiple interactions (structure-band, $df = 12$, $F = 34.39$, $p < 0.0001$; structure-state, $df = 6$, $F = 2.32$, $p = 0.037$; state-band, $df = 8$, $F = 15.17$, $p < 0.0001$; structure-state-band, $df = 24$, $F = 416.35$, $p < 0.0001$). Cortical neurons were more entrained by delta than other frequency bands in the three states (paired t-tests, $t \geq 2.63$, $p \leq 0.018$; df-SWS = 14; df-Task = 21; df-QW = 16). In thalamic cells, this effect was only seen in SWS ($t \geq 7.84$, $p < 0.0001$; $df = 11$) and QW ($t \geq 3.90$, $p \leq 0.005$, $df = 8$) whereas in striatal cells, it was only seen in SWS ($t \geq 4.51$, $p \leq 0.046$; $df = 2$). BLA cells were more entrained by high-gamma than delta in all states ($t \geq 3.97$; $p \leq 0.017$; df-SWS = 4; df-Task = 6; df-QW = 4). **E**, **f**: Correlation of the entrainment values at each frequency between all pairs of simultaneously recorded cortical (**e**) and BLA (**f**) cells. *Within*: pairs of presumed principal cells (P-Cell; cortex, 36,278 pairs; BLA, 17,352 pairs) or fast-spiking interneurons (ITN; cortex, 1,132 pairs; BLA, 2,640 pairs). *Between*: each cell couple includes a principal cell and an interneuron (cortex, 3081 pairs; BLA, 6546 pairs). Mixed-model ANOVA revealed a significant effect of between-subject variables brain structure ($df = 1$, $F = 99.73$, $p < 0.0001$) and state ($df = 2$, $F = 1495.74$, $p < 0.0001$) and of within-subject variable unit identity ($df = 2$, $F = 90.968$, $p < 0.0001$). Variables exhibited multiple interactions (structure-state, $df = 2$, $F = 715.78$, $p < 0.0001$; structure-unit identity, $df = 2$, $F = 45.64$, $p < 0.0001$; state-unit identity, $df = 4$, $F = 8.35$, $p < 0.0001$); structure-state-unit identity, $df = 4$, $F = 9.76$, $p < 0.0001$). In cortical cells, correlation between the frequency profile of unit entrainment was higher in pairs of interneurons than principal cells in all states (rank-sum tests, p's ≤ 2.22e-16) whereas in BLA cells, only during SWS and task performance (p's ≤ 6.69e-9).

values in each state. Kruskal Wallis ANOVAs revealed a significant effect of states in cortical, thalamic, and striatal neurons ($df = 2$, chi-square ≥ 15.6, $p \leq 0.0004$). In cortical and thalamic neurons, post-hoc rank-sum tests indicated a higher correlation in SWS than during QW and task performance (p's ≤ 2.29e-7). By contrast, in striatal cells, the correlation in SWS was lower than during QW ($p = 8.14e\text{-}19$) and task performance ($p = 2.84e\text{-}4$). See legend of Fig. 3 for full statistical details.

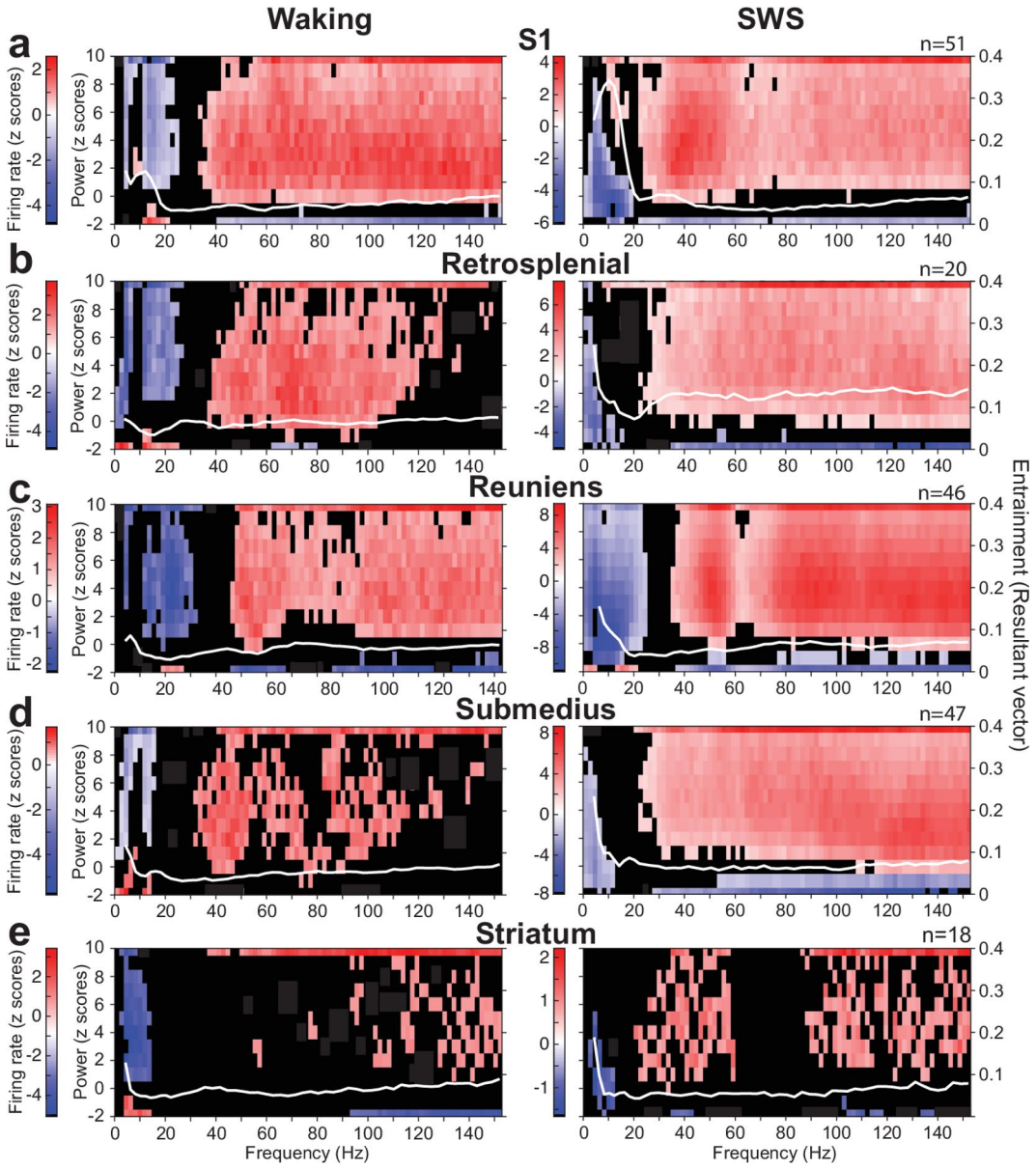

Fig. 3. Relation between firing rate, LFP power, and unit entrainment. Average relation between LFP frequency (x-axis), LFP power (left y-axis), firing rate (color code) and entrainment (white line, right y-axis) during QW (left column) and SWS (right column) in samples of simultaneously recorded cortical (51 S1 cells–**a**; 20 retrosplenial cells–**b**), thalamic (46 reuniens cells - **c**; 47 submedius cells–**d**) and 18 striatal (**e**) neurons. In all cases, we computed LFP power in windows of one second sliding in steps of 200 ms for different frequency bands. The z-scored firing rate of the cells is color coded for each frequency-power bin. The color code is applied only for clusters of ≥ 3 contiguous significant bins. Black indicates non-significant bins. To quantify cell-to-cell variations as a function of states, we correlated the 3D graphs' bin values between all pairs of cells and then compared the distributions of *r* values in each state. Kruskal Wallis ANOVAs revealed a significant effect of states in cortical (df = 2, chi-square = 500.27, $p = 2.33e\text{-}109$; $n = 24{,}777$), thalamic (df = 2, chi-square = 7114.23, $p = 0$; $n = 11{,}608$), and striatal neurons (df = 2, chi-square = 15.6; $p = 0.0004$; $n = 4921$). In cortical neurons, post-hoc rank-sum tests indicated a higher correlation in SWS (0.234 ± 0.005) than during QW (0.106 ± 0.005; $p = 1.73e\text{-}66$) and task performance (0.225 ± 0.003; $p = 2.29e\text{-}7$). Similarly, in thalamic neurons, post-hoc rank-sum tests indicated a higher correlation in SWS (0.752 ± 0.004) than during QW (0.206 ± 0.003; $p = 0$) and task performance (0.313 ± 0.006; $p = 1.84e\text{-}140$). By contrast, in striatal cells, the correlation in SWS (0.040 ± 0.014) was lower than during QW (0.212 ± 0.020; $p = 8.14e\text{-}19$) and task performance (0.159 ± 0.008; $p = 2.84e\text{-}4$).

Individual differences

Superimposed on the general trends described above were marked regional and individual variations. That is, neurons in some regions had exceptionally high entrainment values in particular frequency bands. Depending on the case, these discrepant *R* values were present in only some or all subjects. The latter was the case of neurons in the somatosensory cortex, which had *R* values much higher than typical, between 0.2 and 0.8 in the 8–20 Hz range (Fig. 4a, b), even during task performance in six of six rats. Also, the entrainment of retrosplenial (Fig. 4c, d) and striatal (Fig. 4e, f) neurons to beta oscillations was much higher than in most regions, but this was only seen in one of two or seven rats, respectively. CMT neurons also stood out for their higher than typical entrainment by gamma, but there were marked individual variations in this respect. That is, CMT cells in one rat were preferentially entrained in the high gamma range (~100 Hz, Fig. 4g), cells in three other rats showed a preference for lower gamma frequencies (40–80 Hz), while cells in the remaining rats showed no preferential entrainment to gamma (Fig. 4h).

Overall, the frequency profile of unit entrainment in most structures was not consistent across subjects. To quantify this, we correlated the entrainment profiles of all pairs of available units **w**ithin each **r**at and **s**tructure (WR-WS), **w**ithin each **r**at and **b**etween **s**tructures (WR-BS), **b**etween **r**ats and **w**ithin **s**tructure (BR-WS), and **b**etween **r**ats and **b**etween **s**tructures (BR-BS; Fig. 5). This was done separately for neurons recorded in cortical (anterior cingulate, prelimbic, infralimbic, retrosplenial, subiculum, DP, TT, and S1 areas) and subcortical regions (various midline thalamic nuclei and striatum) but excluding BLA (described below), and in the three states. Similar results were obtained in the two types of neurons and three conditions. A $2\times3\times2\times2$ ANOVA (details in Supplementary Information) revealed significant effects of brain region, behavioral state, unit-structure relationship, and unit-rat relationship ($F \geq 146.96$; $p < 0.0001$) as well as significant bivariate interactions ($F \geq 10.228$; $p < 0.0001$). The variable unit-rat (within vs. between rats) had a much larger effect size (partial eta squared = 0.056) than the other variables (partial eta squared ≤ 0.034). Expectedly, Bonferroni-corrected post-hoc rank-sum tests revealed that in five of the six cases, the average correlation WR-WS was significantly higher than WR-BS (p's < 0.0028 or 0.05/18). However, indicating that the frequency profile of unit entrainment is generally inconsistent across subjects, in all cases, the average correlation BR-WS was significantly lower than WR-BS (p's < 0.0028). Furthermore, differences between correlations BR-WS versus BR-BS had a generally lower magnitude and inconsistent polarity.

Potentially confounding these results however were the varying sample sizes, raising the possibility that they were driven by particular cell types. To test this, we excluded S1 and CMT neurons, which were overrepresented in Fig. 5 (see Table 1). However, the results were unchanged (Fig. S2; statistical details in Supplementary Information). A second concern in Fig. 5a–c is the consideration of cytoarchitecturally heterogeneous cortical areas. Would the same results be obtained if we considered a homogeneous set of regions? To test this, we carried out two control analyses. In the first, we restricted our attention to neurons recorded in the medial prefrontal cortex (infralimbic, prelimbic, and anterior cingulate areas). In the second, we excluded neurons recorded in allocortical areas DP, DTT, and the subiculum. Again, in both cases, the correlations BR-WS were significantly lower than WR-BS while the differences between correlations BR-WS versus BR-BS remained comparatively negligible (Fig. S3; statistical details in Supplementary Information).

A third concern relates to the inclusion of data obtained from male or female rats performing different tasks, each with its specific cognitive and motor demands, and where some subjects were motivated through water versus food restriction. Could inter-individual variations have resulted from these factors? To address this question, we restricted our attention to data obtained in one sex (females, $n = 4$), task (foraging), and restriction type (food), and only considered regions that had been recorded in three or more rats (Fig. 6). Even in these conditions, we obtained the same results as when we combined different tasks, sex, and methods to increase motivation. See Supplementary information for the full statistical analysis. Although we cannot rule out the

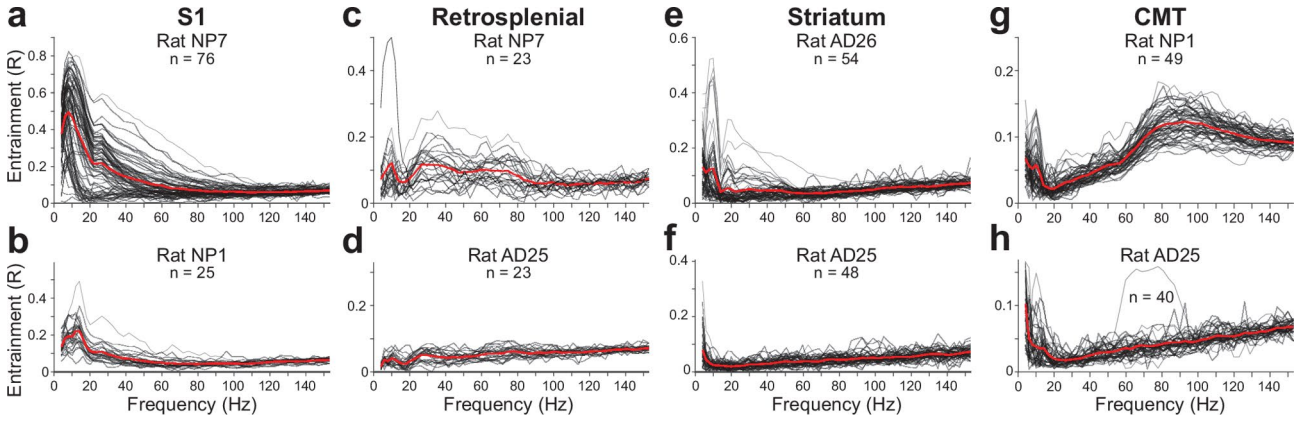

Fig. 4. Individual differences in the frequency profile of unit entrainment. Frequency profile of unit entrainment in (**a**, **b**) S1, (**c**, **d**) retrosplenial, (**e**, **f**) striatal, and (**g**, **h**) central medial thalamic neurons, all recorded during task performance (**a**, **b**,**e**, **f**,**g**, **h** foraging task; **c**, **d**, RRI task). In each case, the data obtained in two distinct rats is displayed. The number of cells included is provided at the top of each panel. Black lines: individual cells. Red lines: average.

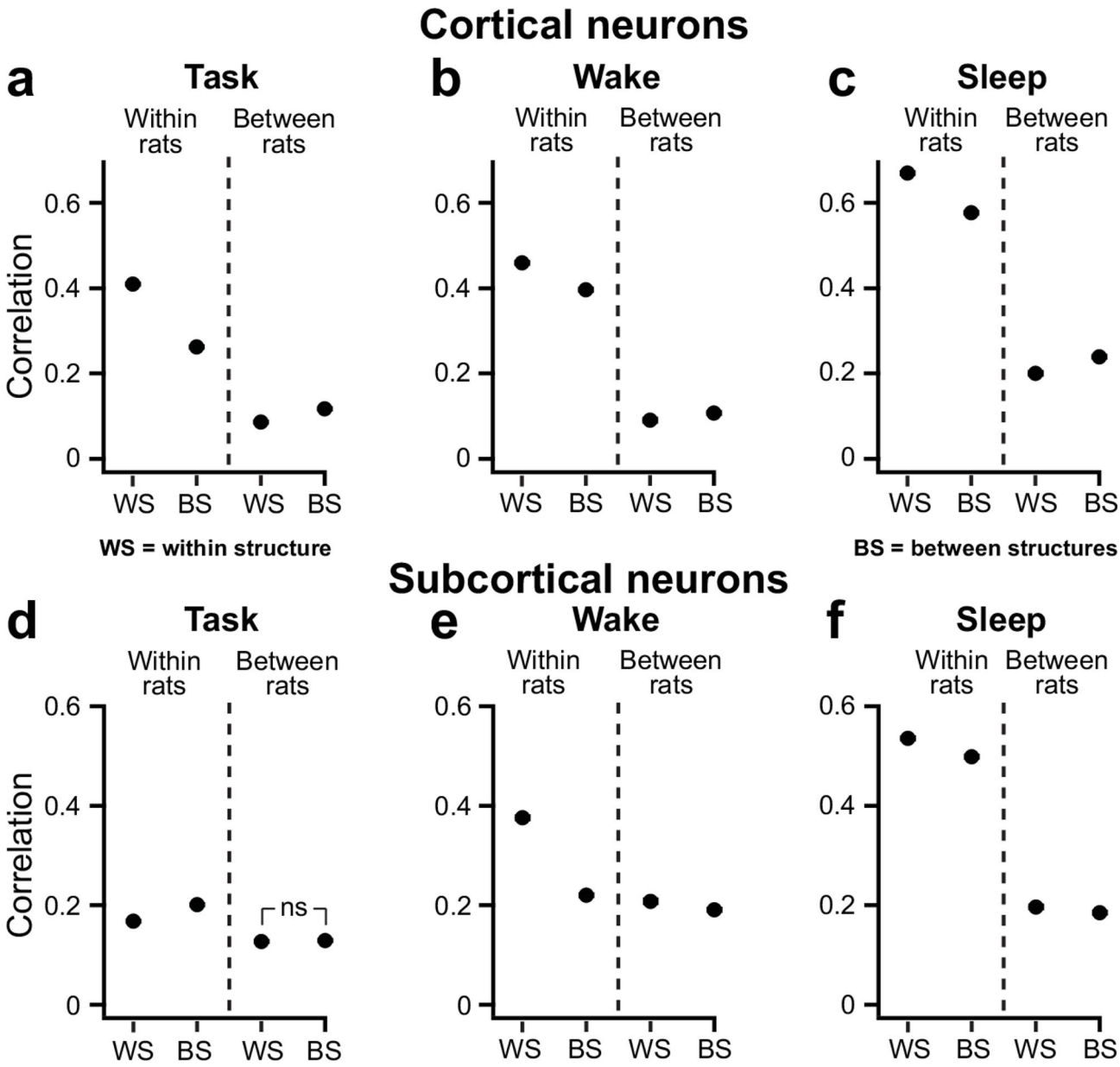

Fig. 5. The frequency profile of unit entrainment is generally inconsistent across subjects. We correlated the entrainment values at each frequency for all available cell pairs in four classes: **w**ithin each **r**at and **w**ithin **s**tructure (WR-WS), **w**ithin each **rat** and **b**etween **s**tructures (WR-BS), **b**etween **r**ats and **w**ithin **s**tructures (BR-WS), or **b**etween **r**ats and **b**etween **s**tructures (BR-BS). We did so separately for cortical (**a**-**c**) and subcortical (**d**,-**f**) neurons, and in three conditions: during performance of the foraging task (**a**, **d**), during QW (**b**, **e**), and SWS (**c**, **f**). We provide the average ± SEM Spearman correlation coefficients (SEMs are so low they are not visible). Number of pairs of cortical cells for task: WR-WS 71,875, WR-BS 55,051, BR-WS 47,325, BR-BS 117,541. Number of pairs of cortical cells for QW and SWS: WR-WS 20,952, WR-BS 19,322, BR-WS 8,664, BR-BS 20,141. Number of pairs of subcortical cells for foraging: WR-WS 224,219, WR-BS 66,509, BR-WS 188,985, BR-BS 226,019. Number of pairs of subcortical cells for QW and SWS: WR-WS 19,078, WR-BS 26,114, BR-WS 7,870, BR-BS 16,838. Abbreviation: ns, not significant.

possibility that differences in the rats' estrous cycle caused some of the inter-individual variability, the fact that we obtained similar results when most of the subjects were males (18 of 23; Fig. 5) argues against this explanation.

BLA neurons stand apart

The sole exception to the pattern of inter-individual heterogeneity was the BLA. Table 2 highlights this by comparing the average correlation between the frequency profiles of unit entrainment BR versus WR in eleven brain regions recorded in two or more rats. Overall, 25 of the 31 WR versus BR comparisons reached significance (rank-sum tests, $p < 0.0015$). In 23 of these 25 comparisons, correlations WR were higher than BR. Contrasting

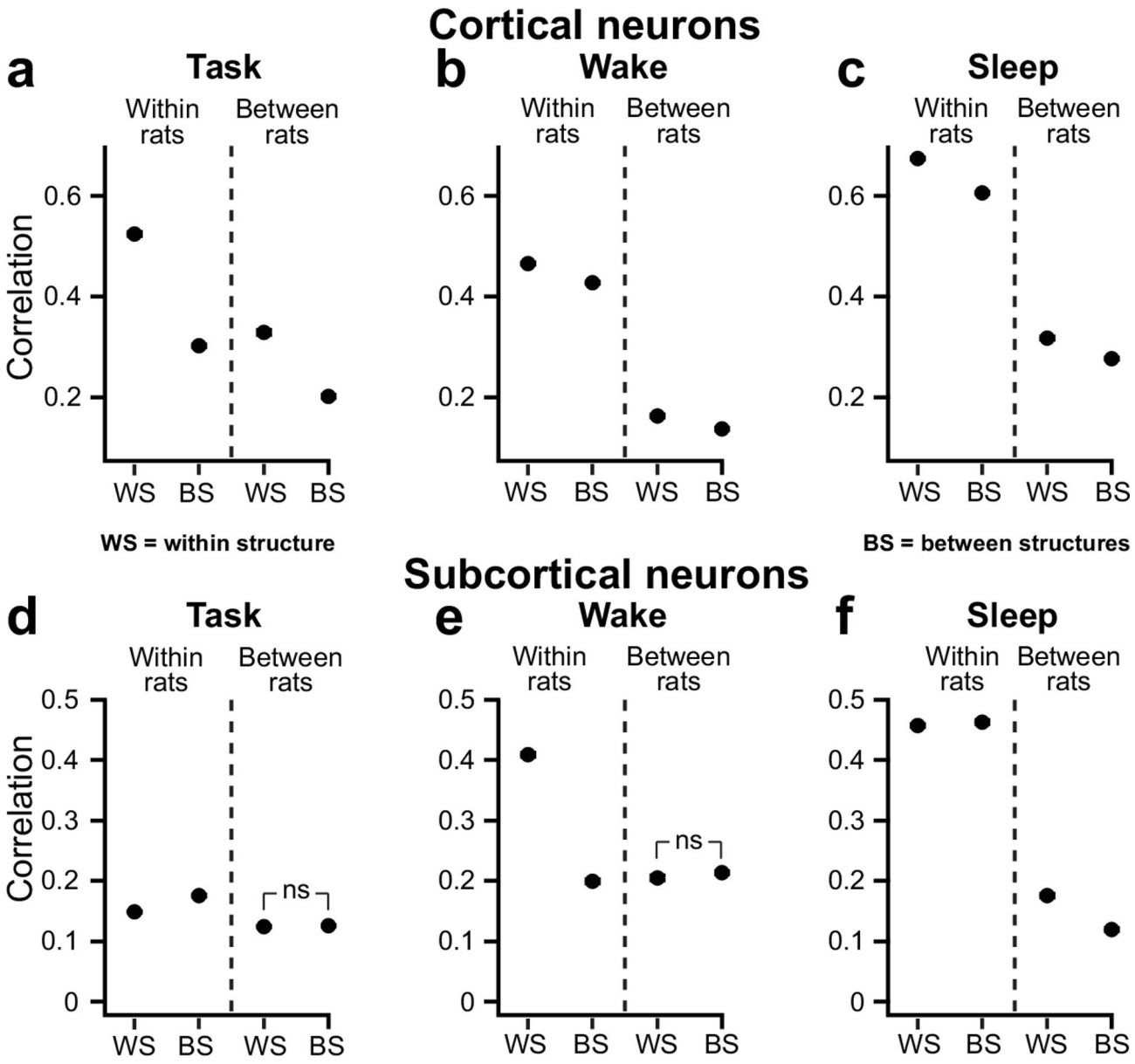

Fig. 6. After eliminating potentially confounding variables, the frequency profile of unit entrainment remains inconsistent across subjects. We carried out the same analysis as in the previous figure except that we only included cells recorded in female rats that performed the foraging task and only considered recording sites for which data was available in at least three rats. We correlated the entrainment values at each frequency for all available cell pairs in four classes: **w**ithin each **r**at and **w**ithin **s**tructure (WR-WS), **w**ithin each **rat** and **b**etween **s**tructures (WR-BS), **b**etween **r**ats and **w**ithin **s**tructures (BR-WS), or **b**etween **r**ats and **b**etween **s**tructures (BR-BS). We did so separately for cortical (**a**-**c**) and subcortical (**d**-**f**) neurons, and in three conditions: during performance of the foraging task (**a**, **d**), during QW (**b**, **e**), and SWS (**c**, **f**). We provide the average ± SEM Pearson correlation coefficients (SEMs are so low they are not visible). Number of cortical cell pairs for the foraging task: WR-WS 12,285, WR-BS 11,446, BR-WS 5,391, BR-BS 11,328. Number of cortical cell pairs for QW and SWS: WR-WS 20,536, WR-BS 17,714, BR-WS 9,607, BR-BS 19,622. Number of subcortical cell pairs for the foraging task: WR-WS 206,575, WR-BS 42,016, BR-WS 176,355, BR-BS 188,035. Number of subcortical cell pairs for QW and SWS: WR-WS 15,181, WR-BS 11,955, BR-WS 6,724, BR-BS 13,566. A $2 \times 3 \times 2 \times 2$ ANOVA revealed significant effects of brain structure, behavioral state, unit-region relationship, and unit-subject relationship ($F \geq 7466.75$; $p < 0.0001$) as well as significant interactions between all these variables ($F \geq 143.13$; $p < 0.0001$). Expectedly, post-hoc rank-sum tests revealed that in four of the six cases, the average correlation WR-WS was significantly higher than WR-BS (p's < 0.0028 or 0.5/18). However, indicating that the frequency profile of unit entrainment is generally inconsistent across subjects, in four of the six cases, the average correlation BR-WS was significantly lower than WR-BS (p's < 0.0028 or 0.5/18). Furthermore, differences between correlations BR-WS versus BR-BS had a generally lower magnitude and inconsistent polarity. Abbreviation: ns, not significant.

	Task					QW					SWS				
	Cells	Rats	WR	BR	p	Cells	Rats	WR	BR	p	Cells	Rats	WR	BR	p
ACg	11	2	0.5232 ± 0.0190	0.3148 ± 0.0373	2.522e-05	80	3	0.3204 ± 0.0036	0.0813 ± 0.0068	5.131e-182	80	3	0.3254 ± 0.0049	0.1594 ± 0.0085	1.745e-60
PL	84	2	0.5692 ± 0.0043	0.2082 ± 0.0051	0	130	3	0.4802 ± 0.0032	0.1294 ± 0.0031	0	130	3	0.8626 ± 0.0012	0.2688 ± 0.0033	0
IL	70	3	0.5917 ± 0.0067	0.2303 ± 0.0056	1.111e-249	69	3	0.4912 ± 0.0055	0.1851 ± 0.0071	9.005e-176	69	3	0.5594 ± 0.0052	0.2372 ± 0.0087	8.543e-173
DP	21	2	0.3803 ± 0.0166	0.4492 ± 0.0243	0.1145	59	2	0.2604 ± 0.0050	0.2173 ± 0.0157	0.0106	59	2	0.4373 ± 0.0050	0.3930 ± 0.0175	0.0063
DTT	14	2	0.4749± 0.0249	0.1318± 0.0376	4.023e-1	18	2	0.5158± 0.0160	0.2894± 0.0321	2.671e-07	18	2	0.7432± 0.0112	0.5471± 0.0243	5.784e-08
S1	101	2	0.4888 ± 0.0056	0.5235 ± 0.0091	0.1090	88	2	0.6955± 0.0042	0.2905 ± 0.0052	0	88	2	0.8913 ± 0.0017	0.6018 ± 0.0048	0
CMT	849	9	0.1389± 6.678e-04	0.1318± 6.826e-04	1.226e-10	132	3	0.4912 ± 0.0030	0.5283 ± 0.0029	3.198e-45	132	3	0.4419 ± 0.0026	0.3221 ± 0.0028	2.063e-161
MDm	57	3	0.2586 ± 0.0060	0.1032 ± 0.0146	5.032e-20	45	3	0.2743 ± 0.0092	0.1321 ± 0.0104	1.490e-20	45	3	0.6017 ± 0.0072	0.2826 ± 0.0082	3.389e-123
SubD	27	4	0.2278 ± 0.0072	0.1792 ± 0.0058	1.671e-05	n/a	n/a	n/a	n/a	n/a	n/a	n/a	n/a	n/a	n/a
CPu	104	3	0.1995 ± 0.0036	0.2162 ± 0.0048	0.0048	112	3	0.1316 ± 0.0061	0.0839 ± 0.0046	4.675e-09	112	3	0.3607 ± 0.0057	0.3113 ± 0.0043	4.109e-09
BLA	324	7	0.2787 ± 0.0024	0.3126 ± 0.0016	4.3563e-17	63	5	0.7607 ± 0.0025	0.7463 ± 0.0014	0.0060	63	5	0.6375 ± 0.0028	0.6325 ± 0.0015	0.5255

Table 2. Correlations between the entrainment values at each frequency for all available cell pairs within (WR) versus between (BR) rats for cell types recorded in ≥ 2 rats. Recording sites are indicated in the left-most column. Three conditions are provided (from left to right): recordings during the foraging task, during quiet wakefulness (QW), and slow-wave sleep (SWS). The significance of the differences WR versus BR were assessed with rank-sum tests. The significance threshold was adjusted for multiple comparisons (0.0015). Overall, 25 of the 31 comparisons reached significance. In 23 of these 25 comparisons, correlations WR were higher than BR. Contrasting with this general pattern, in BLA cells, correlations WR versus BR did not differ in QW and SWS. During task performance, the correlations BR were higher than WR.

with this general pattern, in BLA cells (bottom row), correlations WR versus BR did not differ in QW and SWS. During task performance, the correlations BR were marginally yet significantly higher than WR.

Figure 7a–c illustrates the frequency profile of unit entrainment of three samples of BLA neurons recorded in as many distinct rats during the foraging task. Not only was the entrainment profile similar across the seven rats, but it was stable across days in different samples of BLA neurons recorded in the same rats (Fig. 7d–f). Irrespective of the behavioral state, most BLA neurons showed a preferential entrainment in the same high-gamma frequency range (70–110 Hz) and comparatively little entrainment to low frequencies (Fig. 7g–j).

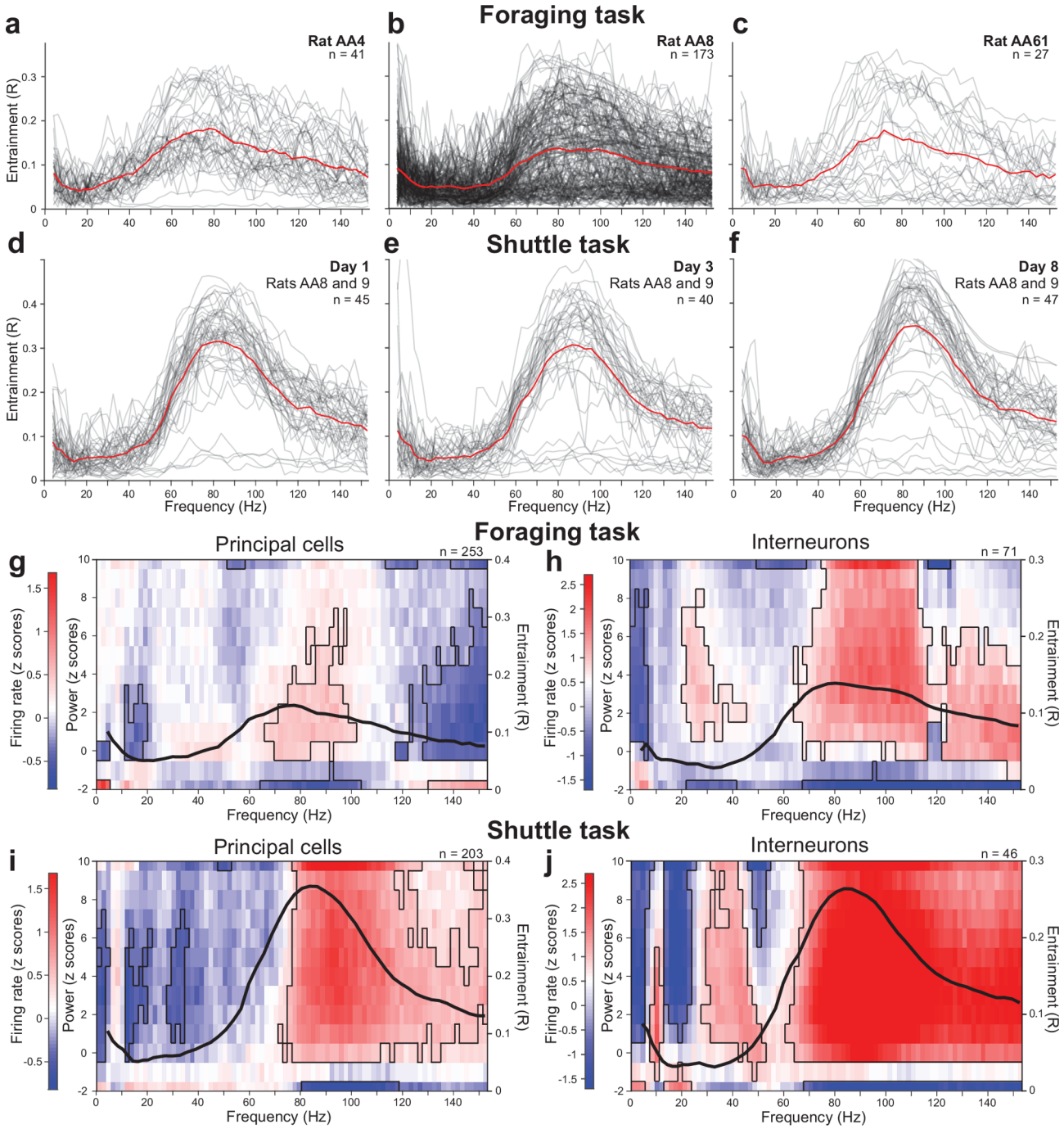

Fig. 7. BLA neurons stand apart. Frequency profile of unit entrainment of BLA neurons recorded during the foraging (**a–c**) and shuttle (**d–f**) tasks. In **a–c**, each panel shows a different sample of BLA neurons recorded in a different rat (labels at top right). In **d–f**, each panel shows a distinct sample of BLA neurons recorded in the same two rats but on different days (labels at top right). (**g–j**) Relation between LFP power (left y-axis), frequency (x-axis), firing rate (color bar), and entrainment (black trace, right y-axis) in presumed principal cells (**g**, **i**) and fast-spiking interneurons (**h**, **j**) of the BLA during the foraging (**g**, **h**) and shuttle (**i**, **j**) tasks.

Although the entrainment profile of BLA units showed a distinct peak in the high-gamma range in all conditions, entrainment magnitude varied significantly across states and tasks (Kruskal-Wallis ANOVA: df = 2, Chi-square = 326.34, $p = 1.37e-71$). That is, average peak R values in the high-gamma range were highest during the shuttle task (0.355 ± 0.007), intermediate during SWS (0.233 ± 0.004), and lowest in the foraging task (0.182 ± 0.006; rank-sum tests, p's < 1.63e-07). Peak frequencies also differed significantly across conditions (Kruskal-Wallis ANOVA: df = 2, Chi-square = 197.58, $p = 1.25e-43$): higher during SWS (103.44 ± 0.87 Hz) than the shuttle (85.4 ± 0.53; rank-sum test, $p = 5.96e-51$) and foraging tasks (90.59 ± 1.33 Hz; rank-sum test, $p = 1.23e-19$), with no difference between the latter two conditions (rank-sum test, $p = 0.89$).

Discussion

Limitations of this study

Because we aimed to determine whether the frequency profile of unit entrainment is a stable property, we considered neuronal activity in three different conditions: during SWS, QW, and task performance. While we conceived the latter as a state of heightened arousal relative to QW, it is likely that analyzing neuronal activity in relation to specific task variables would have revealed that many neuronal populations are transiently entrained at specific frequencies by such variables. However, these phenomena are beyond the scope of the present study. Related to this, our analyses of firing rate and entrainment ignored the potential influence of cross-frequency coupling[5,6]. With phase-amplitude coupling for instance, if some neurons are differentially entrained to the same frequency depending on whether this oscillation is nested in a lower frequency rhythm or not, we may have overlooked phenomena that are consistent across rats.

Another limitation is that our analyses were restricted to a specific subset of cortical areas and subcortical structures. Had we considered other regions, we would likely have encountered additional examples of neurons with distinctive propensities to rhythmic activity. In fact, there are already well documented examples such as inferior olivary neurons firing rhythmically at ~ 10 Hz[22], entorhinal neurons entrained by the theta rhythm[23], and cells in multiple components of the olfactory system displaying gamma rhythmicity[24].

Relation between LFP frequency, entrainment, and firing rates

Cortical, thalamic, and striatal neurons were preferentially entrained by low frequency oscillations. Although this effect was particularly pronounced for the delta band during SWS, it was also observed during QW and task performance. These observations are consistent with prior studies indicating that while delta power is highest in SWS[25], delta oscillations also occur during wakefulness, in relation to various cognitive processes[26,27].

Also consistent with prior reports is the differential relation between firing rates and the power of low versus high-frequency LFP components. Although cortical, thalamic, and striatal neurons were more strongly entrained by low than high LFP frequencies, rises in the power of low (≤ 15 Hz) versus high LFP frequencies were generally associated with decreased versus increased firing rates, respectively. These observations are in keeping with the tight coupling between gamma power and firing rates reported previously[28,29]. They also match current views regarding the origin and cellular correlates of delta oscillations. Indeed, disconnection experiments[30,31] indicate that delta oscillations are generated in the cerebral cortex and synaptically imposed onto thalamic and striatal neurons, explaining why delta oscillations have similar correlates in these different cell types[32–35]. Delta oscillations are associated with reduced firing rates because they consist of alternating periods of depolarization, when they display irregular fast activity in the gamma range, and hyperpolarization, during which neurons are silent[36].

Inter-individual variability

Although neurons recorded simultaneously in a given brain region and behavioral state generally had similar frequency profiles of entrainment, there were pronounced variations between rats. Specifically, neurons in some regions had exceptionally high entrainment values in particular frequency bands but these were not observed consistently across rats. In fact, the correlation between the entrainment profiles of the same type of neurons between rats approximated that of different types of neurons between rats.

While this observation may be perplexing to scientists valuing replicability, it is not surprising. According to Charles River Laboratories, outbred rats like ours "are used in preclinical research to mimic genetic variation in humans" and many studies have shown that brain rhythms have a high heritability[37]. For instance, peak gamma frequencies are more strongly correlated in monozygotic twins ($r = 0.88$) than dizygotic twins ($r = 0.32$) or unrelated subjects ($r = 0.02$;[38]). Moreover, delta, theta, and beta power have a correlation of 0.76 to 0.86 in monozygotic twins compared to − 0.01 to − 0.03 in dizygotic twins[39]. Congruently, human functional imaging and magneto-encephalographic (MEG) studies indicate that patterns of functional connectivity at rest and during task performance are highly variable between subjects but stable over time[40,41]. In fact, these characteristics are so stable that they can be used to identify ("fingerprint") individuals. For instance, a MEG study succeeded in identifying 70% of identical twins based on their functional connectivity patterns during the resting state[42].

Since our rats performed the tasks with similar proficiency despite neurons in different subjects exhibiting distinct oscillatory propensities, what are the implications of our findings for the role of oscillations in brain function? Confronted with this heterogeneity, some might infer that oscillations play a minor role or that different oscillatory patterns can be used to achieve the same result. Alternatively, it is possible that differences in oscillatory propensities affect behavior in a more subtle manner than could be detected with the relatively coarse performance measures we used. Supporting this view, one study reported that differences in cortical entrainment correlate with predictive behavior in sensorimotor synchronization[43]. In this study, the temporal accuracy of movements synchronized with an auditory beat correlated with the amplitude of field responses as seen in the subjects' EEG when they were listening to the beat. Stronger entrainment of the EEG responses was associated with superior temporal prediction abilities. Yet another possibility is that the oscillations critical to

brain function are those we did not investigate here, namely those arising in response to specific task variables or contexts. Perhaps those are less susceptible to genetic variations. Moreover, network oscillations may support the formation of representations by entraining only a minority of neurons from a random sample. While our findings do not allow us to reach a firm conclusion, they do highlight the perils of averaging.

Origin of BLA's high-gamma rhythmicity

An exception to the general pattern of inter-individual heterogeneity we observed was the BLA. Indeed, BLA neurons were more strongly entrained by high-gamma than all other frequency bands and this preference was observed in all subjects, irrespective of behavioral state. Given that different levels of arousal are associated with significant changes in the release of neuromodulators in the BLA[44–47], the mechanisms generating gamma in the BLA must be very robust.

Previously, based on the relative timing of spikes generated by principal cells and presumed interneurons during gamma[15], it was proposed that as in the cerebral cortex, BLA's gamma arises from rhythmic interactions between principal cells and parvalbumin immunoreactive fast-spiking interneurons[48–52]. However, if the same mechanism is operative in the BLA and cortex, why is unit entrainment by spontaneous gamma so much stronger in the BLA? A study comparing the incidence of gamma oscillations in the BLA and lateral nucleus of the amygdala offer some clues[53]. Although these two neighboring nuclei have a cellular composition similar to cortex, only the BLA shows spontaneous gamma. Based on a combination of extracellular recordings and biophysical modeling, the authors concluded that the BLA has a higher propensity to gamma because it has a higher incidence of fast-spiking interneurons and more connections between principal cells and fast-spiking interneurons.

Role of BLA's gamma

Prior studies examined fluctuations in high-gamma power during the foraging[15] and RRI tasks[53]. In the foraging task, high-gamma power increased when rats were apprehensive and decreased when rats-initiated foraging. Congruently, in the RRI task, high-gamma power rose during attentive deliberation or assessment of the environment and then decreased upon behavior initiation. In addition, simultaneous recordings of the BLA and its targets have revealed that the BLA shows coherent gamma with the rhinal cortices[54] and striatum[55] during reward anticipation. Bursts of coherent gamma also occur in the prelimbic cortex[56], a region thought to support higher-order cognitive processes[57,58]. Together, these results suggest that the BLA's high-gamma activity may support response selection and processing of complex stimuli or contingencies.

However, the BLA also displays high-gamma during offline states like SWS and QW. What role could high-gamma play in these circumstances? There is evidence that it facilitates the consolidation of memories for emotionally arousing events. Indeed, a large body of work indicates that the BLA mediates the facilitation of memory by emotions[59,60]. Critically, the BLA is not the storage site of these facilitated memories, but it enhances storage in other brain structures[61,62]. Evidence that the BLA's high-gamma activity is involved in memory consolidation came from a study in which closed-loop optogenetic manipulations that enhanced or dampened high-gamma during memory consolidation respectively facilitated or impaired memory retention[63].

Conclusion

Overall, our results suggest that in many brain regions, the frequency profile of unit entrainment is highly variable across rats. Key challenges for future studies include identifying the factors responsible for these inter-individual variations, testing whether they are present in other rat strains (inbred and outbred), and determining whether they are associated with differences in behavior.

Methods

The present study is reported in accordance with ARRIVE guidelines (https://arriveguidelines.org).

Animals

We used Long-Evans rats of both sexes (5 females, 18 males; RRID: RGD_2308852; 300–350 gm upon delivery; Charles River Laboratories, New Field, NJ) kept on a 12-hour light-dark cycle (lights-off at 7:00 PM). All procedures were carried out during the light phase of the cycle, with the approval of the Institutional Animal Care and Use Committee of Rutgers University, and in compliance with the Guide for the Care and Use of Laboratory Animals. During the first week after delivery, rats had continuous access to water and food. They were then trained on one or two of five behavioral tasks and later implanted with Neuropixel (IMEC, Belgium) or silicon probes (Neuronexus, models 32–64 L, Ann Arbor, MI) in various brain regions.

After recovery from the surgery, rats were retrained until their performance returned to pre-surgical levels, at which point we recorded neuronal activity in three different conditions: during SWS, QW, and task performance (a state of heightened arousal relative to QW). In comparing these three conditions, our goal was to determine whether the frequency profile of unit entrainment is a stable property of the neuronal populations examined, one that transcends behavioral states. As such, the specifics of the tasks we used are not germane to the question investigated here. Nevertheless, the tasks are described succinctly below. However, this paper can be understood without knowledge of the specifics of each task.

Behavior

We used five different behavioral tasks (Fig. 8): the risk reward interaction (RRI) task[64], the foraging task[65,66], the shuttle task[66], the operation task[67] and the expectation control task[68]. In all these tasks, an overhead camera recorded the rats' behavior for off-line analysis. To ensure proper motivation in these tasks, rats had restricted access to food or water during task training and performance. The water restriction protocol, used only in the

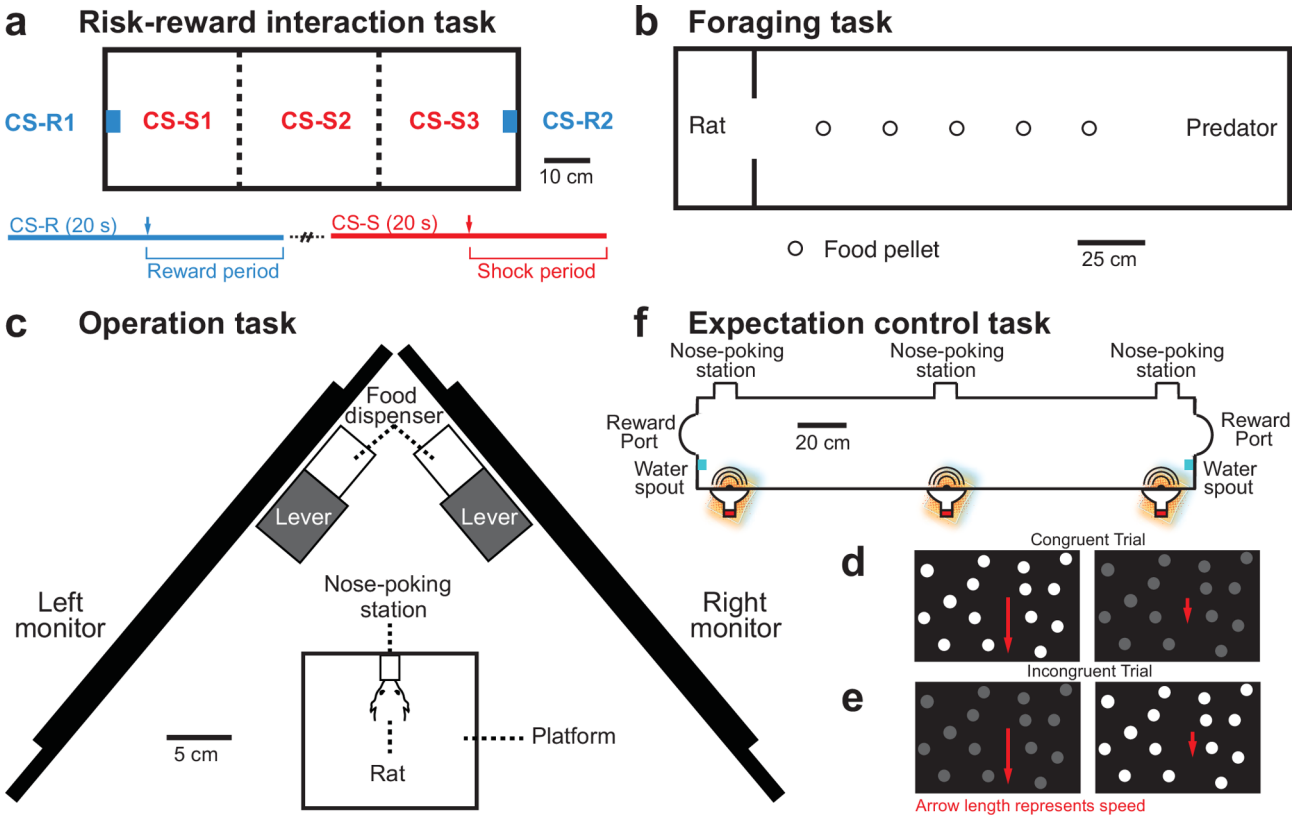

Fig. 8. Behavioral tasks. During the recordings, rats performed one or two of the following tasks. (**a**) Risk-reward interaction task. Top, behavioral apparatus. LED panels behind the water ports and below the floor sectors served as CSs predicting liquid rewards (CS-Rs) and footshocks (CS-Ss), respectively. **Bottom**: trial types. Rats were presented with a random sequence of CS-Rs or CS-Ss. (**b**) Foraging task. The behavioral apparatus featured a dimly lit nest and a longer and brighter foraging arena where rats retrieved food pellets. On half the trial blocks, rats were confronted with a mechanical predator when they ventured in the foraging arena. (**c**) Operation task. Rats were presented with visual stimuli via two computer screens placed on either side of their heads. Rats had to determine on which side the target dimension was highest while ignoring the left-right difference in distractor levels. Rats reported their decision by pressing a lever on the side where the target dimension was higher. Depending on the trial, speed and brightness could be greater on the same side ("*congruent trials*"; **d**) or on opposite sides ("*incongruent trials*"; **e**). (**f**) Expectation control task. Hungry rats ran back and forth between the ends of an elongated arena to obtain food rewards. At each end of the arena was a food reward port and a nose-poking station. A third nose-poking station was placed in the middle of the arena. Rats were trained to nose-poke at one end of the arena and then at the arena's midpoint, each nose-poke triggering the presentation of one of three tones (60 db; 0.7 s) that signaled how many food pellets could be retrieved at the arena's other end.

RRI task, consisted of six days of restriction followed by one day of *ad libitum* access to water while maintaining rats at ≥85% of their initial body weight. In the other tasks, daily access to food was limited in time so that the rats' bodyweight was maintained at about 90% of age-matched subjects with continuous access to food.

Risk reward interaction task

In the RRI task (Fig. 8a), rats could obtain liquid rewards while avoiding footshocks based on light conditioned stimuli (CSs; 20 s) that signaled different outcomes depending on their location. The behavioral apparatus was a dimly lit rectangular arena (90 by 30 cm) with high walls and a floor made of metal bars (5 mm o.d., 8 mm spacing). The floor was divided into three sectors (30 by 30 cm), each with an array of light-emitting diodes (LEDs) below it. At both ends of the apparatus was a water port with LEDs behind it (Fig. 8a). When the CS was presented underneath one of three shock sectors (CS-S; Fig. 8a, red), it indicated that a footshock would be delivered in that sector, 10 s after CS onset. When a light CS was presented behind the left or right wall (CS-R; Fig. 8a, blue), it signaled that a liquid reward would be delivered at that location, 10 s after CS onset. A programmable microcontroller (Arduino, SparkFun, Niwot, CO) determined when and where the LEDs, shocks (0.4 mA, 10 s), and water rewards (60 µl) would be delivered. The CS order was random and the intertrial interval varied between 20 and 40 s. Rats usually reached 80% correct response on all trial types combined after 7–10 days of training. See[64] for additional details.

Shuttle task
In this case, the apparatus was made of black Plexiglas panels (45 cm in height). It was 20 cm in width, 150 cm in length, and divided in three 50 cm compartments, separated by retractable doors. Under dim illumination (10 lx), rats ran back and forth between the ends of the apparatus through the central compartment to retrieve food pellets at the other end. Rats were first habituated to the apparatus with the doors open. When recording, rats were positioned at one of the extremities and a food pellet was placed at the other end. After opening the doors, rats quickly ran to the other end to consume the food. The door was closed while rats consumed the food. The inter-trial interval was ≥ 1 min.

Foraging task
In the foraging task (Fig. 8b[65]), rats are confronted with a mechanical predator when they leave their nest to retrieve food pellets in an elongated arena. See this link for a video clip depicting a rat interacting with the mechanical predator: https://www.youtube.com/watch?v=9AStzt21ZdE. The behavioral apparatus was an elongated alley (245 by 60 cm) with high walls. A sliding door (height, 50 cm; width, 10 cm) subdivided the apparatus into two compartments: a dimly lit (10 lx) nesting area (30 cm) with a water bottle, and a much longer (215 cm) and brighter (200 lx) foraging arena. On each trial, a food pellet (80–100 g) was placed at various distances from the nest (25–150 cm varying in steps of 25 cm). Trials started when the door to the nest was opened. After a variable delay, rats approached the door threshold and stayed there for a while. Eventually, they ventured into the nest, grabbed the food pellet, and ran back to the nest to consume it, at which point the door was closed for one minute. On a proportion of trials, a mechanical predator on wheels (Mindstorms, LEGO systems, Billund, Denmark; length, 34 cm; width, 17 cm; height, 14 cm) was positioned at the end of the foraging arena, facing the nest. It had a sensor that detected the rats' approach, triggering a sudden forward movement (80 cm at 60 cm/sec) and repeated opening and closing of the jaws, after which it returned to its initial position. We conducted alternating blocks of 10–20 predator and no-predator trials for a total of approximately 120 trials per day. See[66] for details.

Operation task
The operation task (Fig. 8c) is a contextual sensory discrimination task in which rats were presented with visual stimuli via two monitors placed on either side of their heads. Rats were trained to select stimuli based on one of two dimensions (brightness or speed) depending on context while the other dimension acted as a distractor (speed or brightness respectively). Two epochs of visual stimulation occurred on each trial: (1) when rats stepped on a platform, triggering the presentation of one of two visual stimuli signaling context, identical on both sides; (2) when rats nose-poked, during which different stimuli to be discriminated were presented via the left and right monitors. The latter varied along two dimensions (speed and brightness; 5 levels each). Rats determined on what side the target dimension was highest, ignoring the left-right difference in distractor levels, and reported their decision by pressing a lever on the side where the target dimension was higher. Depending on trials, speed and brightness could be greater on the same (*congruent trials*; Fig. 8d) or on opposite sides (*incongruent trials*; Fig. 8e). Rats were presented with an 80:20 ratio of incongruent to congruent trials.

Expectation control task
In the expectation control task (Fig. 8f), hungry rats run back and forth in an elongated arena. They are presented with auditory CSs associated with different reward amounts. Rats are trained to nose-poke at one end of the arena, triggering the presentation of one of three tones (CS1; 60 dB; 0.7 s) that signal how many food pellets can be retrieved at the other end (0, 1, or 3 food pellets for tones of 0.5, 4, or 8 kHz, counter-balanced across rats). Rats then run to the arena's midpoint where they must nose-poke a second time, triggering a second tone (CS2), which is either the same (80% of trials) or a different tone (15% of trials) than CS1, confirming or challenging their reward expectations, respectively. Rats manifest their reward expectations through their running speed. During the training phase, reward expectations were never challenged (CS1 and CS2 were always identical). By contrast, during recording sessions, they were challenged on some trials (15% of trials where CS2 differed from CS1). Also, on 5% of trials, rats were presented with noxious white noise (100 dB; 0.7 s).

Surgical methods
After behavioral training, rats were anesthetized with isoflurane, mounted into a stereotaxic apparatus, and their scalp shaven. Rats were administered atropine sulfate (0.05 mg/kg, i.m.) to aid breathing and their scalp was cleansed with Betadine and alcohol. A local anesthetic (Bupivacaine, 0.125% solution, s.c.) was infused along the scalp's midline. Around fifteen minutes later, an incision was made on the midline, cranial muscles were retracted as needed, the skull was cleaned thoroughly, and multiple anchoring titanium screws were placed. A stainless-steel screw was implanted over the cerebellum, which served as ground. Next, burr holes were drilled above the regions of interest and the dura mater was opened. Under stereotaxic guidance, rats were implanted with one or more (up to four) Neuropixel probes or silicon probes. Probes were attached to microdrives and kept in a fixed position throughout the experiments or moved ≥ 100 μm at the end of each daily recording session. See[69] for details regarding the preparation of 3D printed microdrives and headcaps. During the surgeries, body temperature was maintained at 37° C. To reduce post-surgical infection and pain, the antibiotic ointment Neosporin was applied to the wound and the anti-inflammatory drug ketoprofen (2 mg/kg, s.c.) was administered daily for three days.

Recording, LFP processing, and unit clustering
All recordings were obtained after extensive training on one or more of the tasks. Our analyses considered entire behavioral sessions lasting ~ 5 h, including inter-trial intervals. Sleep recordings were performed in nest-

like plexiglass enclosures after behavioral testing. Recordings from passive silicon probes were obtained with 32 to 64 channel analog (Plexon, Dallas, TX) or digital headstages (Intan Technologies, Los Angeles, CA) that sampled signals at 25–30 kHz, respectively. Neuropixel probes with 384 channels were recorded with a PXI-based acquisition card (IMEC, Belgium) controlled with SpikeGLX software (https://github.com/billkarsh/SpikeGLX). The data was stored on hard drives. A notch filter at 60 Hz was applied. Signals were high-pass filtered with a median filter (window of 1.1 ms). To extract action potentials, a threshold was applied to the signal. Principal component analysis was applied on the action potentials and the first three components were clustered using KlustaKwik (http://klustakwik.sourceforge.net/) or Kilosort (https://github.com/MouseLand/Kilosort). Spike clusters were then refined manually using Klusters[70] or SortaSort (https://github.com/dbheadley/SortaSort). Cells with unstable spike shapes were discarded. To be considered, the unit's auto-correlograms had to show a refractory period ≥ 2 ms. Cross-correlograms with refractory periods betrayed sharing of the same unit across clusters; these units were discarded.

To measure spike durations, we used the channel with the maximum peak-to-trough amplitude and measured the peak to trough interval[71]. Cortical and BLA cells were tentatively categorized as presumed principal cells or fast-spiking interneurons based on their spike duration and baseline firing rates. For the BLA, neurons with spike durations > 0.6 ms and firing rates < 6 Hz were considered principal neurons. Neurons with spike durations ≤ 0.6 ms and discharge rates ≥ 6 Hz were classified as fast-spiking interneurons. For cortical cells, neurons firing with spike durations > 0.45 ms were classified as principal neurons. Neurons with spike durations ≤ 0.45 ms and discharge rates ≥ 4 Hz were classified as fast-spiking interneurons. Cortical or BLA cells that did not meet the criteria for principal neurons or fast-spiking interneurons were not considered further.

Local field potential processing and spectral analyses

LFPs were down sampled to 1250–2500 Hz. Spectral analyses were performed using the Chronux spectral analysis MATLAB toolkit (http://chronux.org). We used Chronux's function *mtspecgramc* to calculate a multi-t aper time-frequency spectrogram. The number of tapers was set to 5 and the time-bandwidth product to 3. To compensate for power attenuation with frequency, power was calculated as its natural logarithm. We used a 1 s window sliding in 0.2 s steps. We also tested 400 ms windows sliding in steps of 100 ms and 200 ms windows sliding in steps of 50 ms. The results were qualitatively identical.

In a few cases, the results obtained with the above method were compared with those derived via wavelet decomposition (https://github.com/dbheadley/SimpleWaveletLib.git). In these cases, a family of complex Morlet wavelets (sigma = 15) spanning 1 to 256 Hz in 0.25 octave steps was convolved with the LFP signals and corrected for amplitude inflation at higher frequencies. This yielded spectrograms that covered the entire recording session, sampled every millisecond. Converting the spectrogram to amplitudes was performed by taking the absolute value of the complex spectrogram, while the phase was derived from its angle. To calculate the deviation from $1/f^x$, we log-transformed the amplitude and performed a linear fit to that curve. Subtracting the fitted line revealed the percent change of the spectrum from $1/f^x$. Both methods yielded qualitatively identical results. However, since wavelet decomposition required longer computation times, we report the results obtained with *mtspecgramc*.

Entrainment of unit activity by LFP oscillations

To assess spiking entrainment by LFP oscillations, we related unit activity to LFPs obtained 200 μm from the cell of interest. The direction of the shift between the unit and LFP recording sites varied depending on the type of recording probe (horizontal for silicon probes; vertical for Neuropixel probes). In addition, the neuron's position with respect to the border of the region where it was located influenced the shift's direction: the shift was always toward the center of the recorded region. Hence, the shift could be lateral, medial, dorsal, or ventral. The rationale for using a shift of 200 μm is that the spikes generated by most units are only visible in a few neighboring recording leads, spanning at most 150 μm. Hence, by referring unit activity to LFPs recorded 200 μm away, contamination of the LFP by the unit under consideration is eliminated. In any event, we also conducted controls with higher distances between the unit and LFP recodings sites (400 μm) and the results were qualitatively identical. To determine the cells' entrainment and preferred phase, we bandpass filtered the LFPs in the frequency band of interest with a 2 pole butterworth filter implemented with the *filtfilt* MATLAB function and measured the phase and amplitude at each point by applying a Hilbert transform to the resulting signal. As a result, each spike was assigned a phase. Next, relying on the MATLAB Toolbox for Circular Statistics, we computed the mean resultant vector length for circular data (*circ_r*), a measure of entrainment, the mean phase (*circ_mean*), and determined whether the cell was significantly entrained using a Rayleigh test. The above steps were performed in frequency bins of 2 Hz, from 1 to 22 Hz, and in bins of 3 Hz for higher frequencies. We also examined the results obtained with other frequency binning schemes (2, 5, 10 Hz, bins; 2 Hz bins for frequencies < 13 Hz, 3 Hz bins for the beta range, and 5 Hz bins for higher frequencies) but all binning schemes yielded qualitatively identical results.

Note that because the resultant vector is positively biased with low spike counts, we only considered cells in which at least 10,000 spikes were available. As a control, we compared the results obtained with the above method and the pair-wise phase consistency index[72] and found that the two methods yielded nearly identical results. Last, we also compared the results obtained with a distant versus local LFP reference and found the entrainment results to be very similar.

Relation between firing rate, oscillation power, and frequency

For each cell, LFP power at each frequency was z-scored and stratified in bins of 1 z-score from −2 to 10 z-scores. This process resulted in 1092 frequency-power bins. Then, using a rank-sum test, we compared the actual distribution of firing rates across the one-second windows associated with each frequency-power bin

to that found in all the available one-second time windows. Because the rank-sum test outputs a z statistic that is normally distributed, each frequency-power bin could be associated with a z scored firing rate. After repeating this process for all available cells within a brain region, we averaged the results and compared them to a surrogate distribution obtained as follows. For all cells, we shifted the one-second firing rate windows by a random amount. Then, using a rank-sum test, the shifted firing rate windows of each frequency-power bin were compared to the entire distribution of spike windows. These steps were repeated 100 times and the results averaged. Next, we identified the z value corresponding to a confidence interval of 0.02 (two-tailed) in the 100 shifted distributions and used the MATLAB function *bwconncomp* to identify contiguous clusters of bins greater or below the critical z value in the shifted and actual distributions. Finally, we determined the maximum size of significant clusters (negative or positive) that could be obtained by chance in the shifted distribution, irrespective of position. Clusters of significant bins that exceeded that size in the actual distribution were deemed significant.

Euthanasia and histology

At the end of the experiments, rats were deeply anesthetized with isoflurane. When using silicon probes, small electrolytic lesions (10 μA for 16 s) were made on the most dorsal or ventral electrodes, alternating between shanks, so that the different shanks could be discriminated easily. Localization of Neuropixel probes was facilitated by the fact that their ventral extremity was coated with the fluorescent dye DiI prior to implantation.

In all cases, rats were euthanized with an overdose of isoflurane (inhaled, 4%). After isoflurane abolished all reflexes, when breathing almost stopped, rats were perfused through the heart, first with a saline solution and then a fixative. The brain was then extracted and sliced using a freezing microtome. To help determine the location of silicon probes, brain Sect. (80 μm) were counterstained with thionine. For Neuropixel probes, brain sections were first observed with a fluorescence microscope and photographed. The coverslip of the sections containing the probes were then removed and the sections counterstained with thionine.

Statistical analyses

Statistical analyses were performed with MATLAB and SPSS. Data are reported as means ± standard errors. All statistical tests are two-sided. For all analyses, we provide the sample sizes (e.g. number of recording sites, single units), degrees of freedom, and effect sizes. No data was excluded.

State-dependence of unit entrainment

To assess the state-dependence of unit entrainment, we averaged entrainment values of each unit in the delta (1–4 Hz), theta (5–12 Hz), beta (13–30 Hz), low-gamma (31–65 Hz), and high-gamma (66–100 Hz) bands in three different states separately (SWS, QW, task performance). We ran a mixed-model ANOVA with brain structure (BLA, cortex, striatum, thalamus) and behavioral state (QW, SWS, task) as between-subject variables and frequency band (delta, theta, beta, low-gamma, high-gamma) as a within-subject variable. We used Tukey's post-hoc analysis to study the effects of each of the between-subject variables (brain structure, behavioral state) on the rest of the variables. Based on the significant interactions between behavioral states and frequency bands across all brain structures, we used paired-samples t-tests to conduct post-hoc analyses on the difference in entrainment between various frequency bands within specific brain structures and behavioral states.

Comparison between the entrainment profile of presumed principal cells and interneurons

We used multifactorial ANOVAs to analyze the correlation coefficients of within- and between-unit activity in different behavioral states. We tested the effects of brain structure (BLA, cortex), behavioral state (QW, SWS, task), and unit comparison (between-principal cells and interneurons, within-interneurons, within-principal cells) as between-subject variables. We used Tukey's post-hoc analysis to study the effects of each of the between-subject variables (brain structure, behavioral state) on the other variables.

Quantification of heterogeneity in the relation between firing rate and entrainment across behavioral states

To quantify this heterogeneity, we correlated all bin values in the 3D graphs (z values returned by the rank-sum test) between all pairs of available cells. We then assessed the influence of behavioral states (SWS, QW, task) by computing a Kruskal Wallis ANOVA on the distributions of *r* values in each state, followed by Bonferroni-corrected post-hoc rank-sum tests comparing individual states.

Quantifying individual differences in the frequency profile of unit entrainment

To quantify inter-individual heterogeneity, we correlated the entrainment profiles of all pairs of available units in four conditions: **w**ithin each **r**at and **s**tructure (WR-WS), **w**ithin each **r**at and **b**etween **s**tructures (WR-BS), **b**etween **r**ats and **w**ithin **s**tructure (BR-WS), and **b**etween **r**ats and **b**etween **s**tructures (BR-BS), in three states (SWS, QW, task). We used a multifactorial $2 \times 3 \times 2 \times 2$ ANOVA to analyze the correlation coefficients of within- and between-unit activity in different behavioral states. We tested the effects of brain structure (cortex, subcortex), behavioral state (awake, asleep, task), unit-region relationship (within-region, between-region), and unit-subject relationship (within-subject, between-subject) as between-subject variables. We used Tukey's post-hoc analysis to study the effects of each of the between-subject variables. Last, we used Bonferroni-corrected post-hoc rank-sum tests to compare the correlations WR-WS, WR-BS, BR-WS, and BR-BS.

Data availability

The full dataset has not been deposited in a public repository because of its size but is available from the corresponding author upon request.

Received: 30 August 2024; Accepted: 7 January 2025

Published online: 13 January 2025

References

1. Buzsáki, G. *Rhythms of the Brain* (Oxford University Press, 2006). https://doi.org/10.1093/acprof:oso/9780195301069.001.0001
2. He, B. J., Snyder, A. Z., Zempel, J. M., Smyth, M. D. & Raichle, M. E. Electrophysiological correlates of the brain's intrinsic large-scale functional architecture. *Proc. Natl. Acad. Sci. U. S. A.* 105, 16039–16044 (2008).
3. Buzsáki, G., Logothetis, N. & Singer, W. Scaling brain size, keeping timing: evolutionary preservation of brain rhythms. *Neuron* **80**, 751–764 (2013).
4. Fries, P. Rhythms for cognition: Communication through coherence. *Neuron* **88**, 220–235 (2015).
5. Canolty, R. T. & Knight, R. T. The functional role of cross-frequency coupling. *Trends Cogn. Sci.* **14**, 506–515 (2010).
6. Belluscio, M. A., Mizuseki, K., Schmidt, R., Kempter, R. & Buzsáki, G. Cross-frequency phase–phase coupling between theta and gamma oscillations in the hippocampus. *J. Neurosci.* **32**, 423–435 (2012).
7. Hutcheon, B. & Yarom, Y. Resonance, oscillation and the intrinsic frequency preferences of neurons. *Trends Neurosci.* **23**, 216–222 (2000).
8. Llinás, R. R. The intrinsic electrophysiological properties of mammalian neurons: Insights into central nervous system function. *Science* **242**, 1654–1664 (1988).
9. McCormick, D. A. & Pape, H. C. Properties of a hyperpolarization-activated cation current and its role in rhythmic oscillation in thalamic relay neurones. *J. Physiol.* **431**, 291–318 (1990).
10. Steriade, M., McCormick, D. A. & Sejnowski, T. J. Thalamocortical oscillations in the sleeping and aroused brain. *Science* **262**, 679–685 (1993).
11. Pare, D., Pape, H. C. & Dong, J. Bursting and oscillating neurons of the cat basolateral amygdaloid complex in vivo: Electrophysiological properties and morphological features. *J. Neurophysiol.* **74**, 1179–1191 (1995).
12. Pape, H. C., Paré, D. & Driesang, R. B. Two types of intrinsic oscillations in neurons of the lateral and basolateral nuclei of the amygdala. *J. Neurophysiol.* **79**, 205–216 (1998).
13. Ehrlich, D. E., Ryan, S. J. & Rainnie, D. G. Postnatal development of electrophysiological properties of principal neurons in the rat basolateral amygdala. *J. Physiol.* **590**, 4819–4838 (2012).
14. Ryan, S. J. et al. Spike-timing precision and neuronal synchrony are enhanced by an interaction between synaptic inhibition and membrane oscillations in the amygdala. *PLoS ONE.* **7**, e35320 (2012).
15. Amir, A., Headley, D. B., Lee, S. C., Haufler, D. & Paré, D. Vigilance-associated gamma oscillations coordinate the ensemble activity of basolateral amygdala neurons. *Neuron* **97**, 656–669e7 (2018).
16. Hájos, N. Interneuron types and their circuits in the Basolateral amygdala. *Front Neural Circuits* **15**, (2021).
17. Rainnie, D. G., Mania, I., Mascagni, F. & McDonald, A. J. Physiological and morphological characterization of parvalbumin-containing interneurons of the rat basolateral amygdala. *J. Comp. Neurol.* **498**, 142–161 (2006).
18. Woodruff, A. R. & Sah, P. Networks of parvalbumin-positive interneurons in the basolateral amygdala. *J. Neurosci.* **27**, 553–563 (2007).
19. Spampanato, J., Polepalli, J. & Sah, P. Interneurons in the basolateral amygdala. *Neuropharmacology* **60**, 765–773 (2011).
20. Zanos, T. P., Mineault, P. J. & Pack, C. C. Removal of spurious correlations between spikes and local field potentials. *J. Neurophysiol.* **105**, 474–486 (2011).
21. Scheffer-Teixeira, R., Belchior, H., Leão, R. N., Ribeiro, S. & Tort, A. B. L. On high-frequency field oscillations (>100 hz) and the spectral leakage of spiking activity. *J. Neurosci.* **33**, 1535–1539 (2013).
22. Lang, E. J., Sugihara, I., Welsh, J. P. & Llinás, R. Patterns of spontaneous purkinje cell complex spike activity in the awake rat. *J. Neurosci.* **19**, 2728–2739 (1999).
23. Newman, E. L. & Hasselmo, M. E. Grid cell firing properties vary as a function of theta phase locking preferences in the rat medial entorhinal cortex. *Front Syst. Neurosci* **8**, (2014).
24. Kay, L. M. Olfactory system oscillations across phyla. *Curr. Opin. Neurobiol.* **31**, 141–147 (2015).
25. Steriade, M. & Hobson, J. A. Neuronal activity during the sleep-waking cycle. *Prog Neurobiol.* **6**, 157–376 (1976).
26. Harmony, T. The functional significance of delta oscillations in cognitive processing. *Front Integr. Neurosci* **7**, (2013).
27. Nácher, V., Ledberg, A., Deco, G. & Romo, R. Coherent delta-band oscillations between cortical areas correlate with decision making. *Proc. Natl. Acad. Sci. U S A.* **110**, 15085–15090 (2013).
28. Mukamel, R. et al. Coupling between neuronal firing, field potentials, and fMRI in human auditory cortex. *Science* **309**, 951–954 (2005).
29. Nir, Y. et al. Coupling between neuronal firing rate, gamma LFP, and BOLD fMRI is related to interneuronal correlations. *Curr. Biol.* **17**, 1275–1285 (2007).
30. Steriade, M., Nunez, A. & Amzica, F. Intracellular analysis of relations between the slow (<1 hz) neocortical oscillation and other sleep rhythms of the electroencephalogram. *J. Neurosci.* **13**, 3266–3283 (1993).
31. Timofeev, I. & Steriade, M. Low-frequency rhythms in the thalamus of intact-cortex and decorticated cats. *J. Neurophysiol.* **76**, 4152–4168 (1996).
32. Steriade, M., Contreras, D., Curró Dossi, R. & Nuñez, A. The slow (<1 hz) oscillation in reticular thalamic and thalamocortical neurons: Scenario of sleep rhythm generation in interacting thalamic and neocortical networks. *J. Neurosci. Off J. Soc. Neurosci.* **13**, 3284–3299 (1993).
33. Wilson, C. J. & Groves, P. M. Spontaneous firing patterns of identified spiny neurons in the rat neostriatum. *Brain Res.* **220**, 67–80 (1981).
34. Wilson, C. & Kawaguchi, Y. The origins of two-state spontaneous membrane potential fluctuations of neostriatal spiny neurons. *J. Neurosci.* **16**, 2397–2410 (1996).
35. Mahon, S. et al. Distinct patterns of striatal medium spiny neuron activity during the natural sleep-wake cycle. *J. Neurosci. Off J. Soc. Neurosci.* **26**, 12587–12595 (2006).
36. Steriade, M., Nunez, A. & Amzica, F. A novel slow (<1 hz) oscillation of neocortical neurons in vivo: depolarizing and hyperpolarizing components. *J. Neurosci.* **13**, 3252–3265 (1993).
37. van Beijsterveldt, C. E. M. & van Baal, G. C. M. Twin and family studies of the human electroencephalogram: A review and a meta-analysis. *Biol. Psychol.* **61**, 111–138 (2002).
38. van Pelt, S., Boomsma, D. I. & Fries, P. Magnetoencephalography in twins reveals a strong genetic determination of the peak frequency of visually induced γ-band synchronization. *J. Neurosci. Off J. Soc. Neurosci.* **32**, 3388–3392 (2012).
39. Lykken, D. T., Tellegen, A. & Thorkelson, K. Genetic determination of EEG frequency spectra. *Biol. Psychol.* **1**, 245–259 (1974).
40. Dimitriadis, S. I., Routley, B., Linden, D. E. J. & Singh, K. D. Multiplexity of human brain oscillations as a personal brain signature. *Hum. Brain Mapp.* **44**, 5624–5640 (2023).
41. Finn, E. S. et al. Functional connectome fingerprinting: Identifying individuals using patterns of brain connectivity. *Nat. Neurosci.* **18**, 1664–1671 (2015).
42. Demuru, M. et al. Functional and effective whole brain connectivity using magnetoencephalography to identify monozygotic twin pairs. *Sci. Rep.* **7**, 9685 (2017).
43. Nozaradan, S., Peretz, I. & Keller, P. E. Individual differences in rhythmic cortical entrainment correlate with predictive behavior in sensorimotor synchronization. *Sci. Rep.* **6**, 20612 (2016).

44. Hori, K., Tanaka, J. & Nomura, M. Effects of discrimination learning on the rat amygdala dopamine release: A microdialysis study. *Brain Res.* **621**, 296–300 (1993).
45. Tanaka, T. et al. Noradrenaline release in the rat amygdala is increased by stress: Studies with intracerebral microdialysis. *Brain Res.* **544**, 174–176 (1991).
46. Kawahara, H., Yoshida, M., Yokoo, H., Nishi, M. & Tanaka, M. Psychological stress increases serotonin release in the rat amygdala and prefrontal cortex assessed by in vivo microdialysis. *Neurosci. Lett.* **162**, 81–84 (1993).
47. McIntyre, C. K., Marriott, L. K. & Gold, P. E. Cooperation between memory systems: Acetylcholine release in the amygdala correlates positively with performance on a hippocampus-dependent task. *Behav. Neurosci.* **117**, 320–326 (2003).
48. Csicsvari, J., Jamieson, B., Wise, K. D. & Buzsáki, G. Mechanisms of gamma oscillations in the hippocampus of the behaving rat. *Neuron* **37**, 311–322 (2003).
49. Cardin, J. A. et al. Driving fast-spiking cells induces gamma rhythm and controls sensory responses. *Nature* **459**, 663–667 (2009).
50. Sohal, V. S., Zhang, F., Yizhar, O. & Deisseroth, K. Parvalbumin neurons and gamma rhythms enhance cortical circuit performance. *Nature* **459**, 698–702 (2009).
51. Otte, S., Hasenstaub, A. & Callaway, E. M. Cell type-specific control of neuronal responsiveness by gamma-band oscillatory inhibition. *J. Neurosci.* **30**, 2150–2159 (2010).
52. Hasenstaub, A., Otte, S. & Callaway, E. Cell type-specific control of spike timing by gamma-band oscillatory inhibition. *Cereb. Cortex*. **bhv044** https://doi.org/10.1093/cercor/bhv044 (2015).
53. Headley, D. B., Kyriazi, P., Feng, F., Nair, S. S. & Pare, D. Gamma oscillations in the basolateral amygdala: Localization, microcircuitry, and behavioral correlates. *J. Neurosci.* **41**, 6087–6101 (2021).
54. Bauer, E. P., Paz, R. & Paré, D. Gamma oscillations coordinate amygdalo-rhinal interactions during learning. *J. Neurosci. Off J. Soc. Neurosci.* **27**, 9369–9379 (2007).
55. Popescu, A. T., Popa, D. & Paré, D. Coherent gamma oscillations couple the amygdala and striatum during learning. *Nat. Neurosci.* **12**, 801–807 (2009).
56. Stujenske, J. M., Likhtik, E., Topiwala, M. A. & Gordon, J. A. Fear and safety engage competing patterns of theta-gamma coupling in the basolateral amygdala. *Neuron* **83**, 919–933 (2014).
57. Fusi, S., Miller, E. K. & Rigotti, M. Why neurons mix: High dimensionality for higher cognition. *Curr. Opin. Neurobiol.* **37**, 66–74 (2016).
58. Kyriazi, P., Headley, D. B. & Paré, D. Different multidimensional representations across the amygdalo-prefrontal network during an approach-avoidance task. *Neuron* **107**, 717–730e5 (2020).
59. McGaugh, J. L. Memory–a century of consolidation. *Science* **287**, 248–251 (2000).
60. Paré, D. & Headley, D. B. The amygdala mediates the facilitating influence of emotions on memory through multiple interacting mechanisms. *Neurobiol. Stress.* **24**, 100529 (2023).
61. Packard, M. G., Cahill, L. & McGaugh, J. L. Amygdala modulation of hippocampal-dependent and caudate nucleus-dependent memory processes. *Proc. Natl. Acad. Sci.* 91, 8477–8481 (1994).
62. Wahlstrom, K. L. et al. Basolateral amygdala inputs to the medial entorhinal cortex selectively modulate the consolidation of spatial and contextual learning. *J. Neurosci.* **38**, 2698–2712 (2018).
63. Kanta, V., Pare, D. & Headley, D. B. Closed-loop control of gamma oscillations in the amygdala demonstrates their role in spatial memory consolidation. *Nat. Commun.* **10**, (2019).
64. Kyriazi, P., Headley, D. B. & Pare, D. Multi-dimensional coding by basolateral amygdala neurons. *Neuron* **99**, 1315–1328e5 (2018).
65. Choi, J. S. & Kim, J. J. Amygdala regulates risk of predation in rats foraging in a dynamic fear environment. *Proc. Natl. Acad. Sci.* 107, 21773–21777 (2010).
66. Amir, A., Lee, S. C., Headley, D. B., Herzallah, M. M. & Pare, D. Amygdala signaling during foraging in a hazardous environment. *J. Neurosci.* **35**, 12994–13005 (2015).
67. Amir, A. et al. Washington DC,. Coding by medial prefrontal neurons is not random, but respects the logic of a contextual visual discrimination task. in (2023).
68. Gomez-Alatorre, L. F., Amir, A., Karki, A., Herzallah, M. M. & Paré, D. Signaling of salience and prediction errors by the anterior insula. in (2023).
69. Headley, D. B., DeLucca, M. V., Haufler, D. & Paré, D. Incorporating 3D-printing technology in the design of head-caps and electrode drives for recording neurons in multiple brain regions. *J. Neurophysiol.* **113**, 2721–2732 (2015).
70. Hazan, L., Zugaro, M., Buzsáki, G. & Klusters NeuroScope, NDManager: A free software suite for neurophysiological data processing and visualization. *J. Neurosci. Methods*. **155**, 207–216 (2006).
71. Barthó, P. et al. Characterization of neocortical principal cells and interneurons by network interactions and extracellular features. *J. Neurophysiol.* **92**, 600–608 (2004).
72. Vinck, M., van Wingerden, M., Womelsdorf, T., Fries, P. & Pennartz, C. M. A. The pairwise phase consistency: A bias-free measure of rhythmic neuronal synchronization. *NeuroImage* **51**, 112–122 (2010).
73. Herzallah, M. M., Amir, A. & Paré, D. Influence of rat central thalamic neurons on foraging behavior in a hazardous environment. *J. Neurosci.* **42**, 6053–6068 (2022).

Acknowledgements

This work was supported by R01 grants MH130331 and MH119854 to DP from NIMH. MB, ITK, and LFGA were supported by the Neuroscience Graduate Program of Rutgers University - Newark.

Author contributions

D.P. and M.B. conceived the project. I.T.K., A.A., D.B.H., M.H., and L.A. carried out the experiments. All authors contributed to the data analysis. D.P. and M.B. prepared the figures. DP wrote the first draft of the manuscript. All authors contributed to refine the manuscript.

Declarations

Competing interests

The authors declare no competing interests.

Additional information

Supplementary Information The online version contains supplementary material available at https://doi.org/10.1038/s41598-025-85914-2.

Correspondence and requests for materials should be addressed to D.P.